

Ocean Surface Impacts on the Seasonal-Mean Precipitation over the Tropical Indian Ocean

MINGYUE CHEN, WANQIU WANG, AND ARUN KUMAR

Climate Prediction Center, NOAA/NWS/NCEP, Camp Springs, Maryland

HUI WANG AND BHASKAR JHA

Climate Prediction Center, NOAA/NWS/NCEP, Camp Springs, Maryland, and WYLE Information Systems, McLean, Virginia

(Manuscript received 14 June 2011, in final form 18 November 2011)

ABSTRACT

This study analyzes factors affecting the predictability of seasonal-mean precipitation over the tropical Indian Ocean. The analysis focuses on the contributions from the local sea surface temperature (SST) forcing in the Indian Ocean, the remote SST forcing related to ENSO in the tropical eastern Pacific, and the role of local air–sea coupling. To understand the impacts of the individual factors, the prediction skill over the tropical Indian Ocean for four model simulations, but with different treatments for the ocean, are compared. The seasonality in precipitation skill, the local precipitation–SST relationship, and prediction skill related to Indian Ocean dipole mode (IODM) are examined. It is found that the importance of the accuracy of local SST and the presence of local air–sea coupling in the Indian Ocean has a strong seasonal dependence. Accurate local SSTs are important during the boreal fall season, whereas the local air–sea coupling is important during the boreal spring. The precipitation skill over the Indian Ocean during boreal winter is primarily from ENSO. However, ENSO impacts are better realized with the inclusion of an interactive ocean. For all four seasons, the simulation without the interannual variations of local SST in the Indian Ocean shows the least precipitation skill and a much weaker seasonality. It is also found that, for the simulation where the global SSTs are relaxed to the observations and hence maintain some level of active air–sea coupling, the observed seasonal cycle of precipitation–SST relationship is reproduced reasonably well. In addition, the analysis also shows that simulations with accurate SST forcing display high precipitation skill during strong IODM events, indicating that IODM SST acts as a forcing for the atmospheric variability.

1. Introduction

Understanding the mechanisms controlling the interannual variability of seasonal-mean precipitation and its predictability is important because precipitation in the tropics (i) represents the atmospheric latent heat release that is an important component in the global energy balance; (ii) influences the global and regional hydrological cycle; (iii) is closely related to the predictability of seasonal-mean large-scale circulation and its influence on high-frequency systems such as the tropical cyclone variability; and (iv) is one of the dominant atmospheric

signatures of variability related to the El Niño–Southern Oscillation (ENSO), with significant impacts over the global climate (Webster et al. 1998; Wang et al. 2001; Yu et al. 2002; Wu and Kirtman 2004; Annamalai et al. 2005). In addition, tropical precipitation is also one of the forcing components that drive the oceanic circulation by affecting subsurface vertical density stratification through changes in the freshwater budget and salinity.

Over a particular region, interannual variability of precipitation can have several controlling factors. The occurrence of tropical deep convection depends on the warmth of ocean surface and, in general, colder sea surface temperatures (SSTs) are not conducive for precipitation (Zhang 1993). Therefore, interannual variations in SSTs can influence the local precipitation variability. An example of this is the precipitation variability in the tropical eastern Pacific associated with ENSO SST variability

Corresponding author address: Mingyue Chen, CPC, NOAA/NWS/NCEP, 5200 Auth Road, Room 605, Camp Springs, MD 20746.

E-mail: mingyue.chen@noaa.gov

(Arakawa and Kitoh 2004; Trenberth and Shea 2005). Further, because global mass flux across a pressure surface is conserved, regions of enhanced precipitation with upward mass flux are also associated with regions of suppressed precipitation with downward motion elsewhere leading to nonlocal reduction in precipitation. As a consequence, interannual variation in precipitation can also be caused by precipitation changes in remote regions via the atmospheric bridge (Alexander et al. 2002). Understanding interannual variability in precipitation over a region therefore requires understanding various controlling mechanisms. In this paper, our focus is on the analysis of the interannual variability over the Indian Ocean. Although the precipitation variability over the tropical Pacific has been widely studied and is well understood to be tightly controlled by the local SST variability associated with ENSO, the precipitation variability over the Indian Ocean is posited to be due to multiple factors. To provide further motivation for our analysis, below we first summarize various possible mechanisms for precipitation variability over the Indian Ocean.

It is well known that anomalous SST associated with ENSO is the primary source of the seasonal predictability of global circulation (Shukla and Wallace 1983; Brankovic et al. 1994; Livezey et al. 1996; Barnett et al. 1997; Kumar and Hoerling 1998; Kumar et al. 2003; Schubert et al. 2008). Many earlier observational and numerical modeling studies have shown that ENSO SST in tropical Pacific also has a strong remote influence on the atmospheric and SST variability over the Indian Ocean through the atmospheric bridge (Klein et al. 1999; Alexander et al. 2002; B. Wang et al. 2005; Wu and Kirtman 2005; Krishna Kumar et al. 2005; Wu et al. 2008). However, it is still not clear to what extent the remote SST forcing associated with ENSO contributes directly (via changes in atmospheric circulation) or indirectly (via changes in SST) to the seasonal-mean precipitation variability over the Indian Ocean.

In tropical oceans, higher SSTs, in general, are accompanied by increased convection and precipitation (Zhang 1993). For example, over the equatorial tropical Pacific, the interannual variation of precipitation is positively correlated with the underlying SST variability, implying warm SST leading to an increase in precipitation. The positive correlation is highest in the tropical eastern Pacific where the amplitude of interannual SST variation associated with ENSO is also the largest (Arakawa and Kitoh 2004; Trenberth and Shea 2005; Wu et al. 2006). This strong positive relationship reflects the influence of SST forcing and is a major contributor to the prediction skill for tropical precipitation. The controlling influence of SST over this region is also confirmed by successful simulations of interannual variability of precipitation with

atmospheric general circulation models (AGCMs) with specified SST forcing (e.g., Shukla and Wallace 1983; Kang et al. 2002; Wang et al. 2004; Peng and Kumar 2005; Peng et al. 2009).

Interannual variability of SST over the tropical Indian Ocean is weaker than that over the tropical eastern Pacific, and also the control of SST on precipitation is not as well understood. Previous studies have shown that the precipitation anomalies have a weak negative correlation with the underlying SST anomalies over the north Indian Ocean and western North Pacific in boreal summer (Trenberth and Shea 2005; B. Wang et al. 2005; Wu et al. 2006). A negative SST–precipitation correlation implies that the coupled air–sea interaction in these regions such that SSTs respond to atmospheric variability. The seasonality, as well as spatial dependence, of precipitation–SST correlation over the Indian Ocean, however, is not well documented or understood.

Another aspect related to the precipitation variability over the Indian Ocean is the role of the coupled air–sea interaction. In numerical model studies, it is found that coupled simulations have a better depiction of the relationship between SST and precipitation variability over the Indian monsoon region than that simulated in AGCM-alone simulations with specified SST forcing; that is, the Atmospheric Model Intercomparison Project (AMIP) type of simulations (B. Wang et al. 2005; Wu and Kirtman 2005; Krishna Kumar et al. 2005; Wu et al. 2006). Most of the previous studies have focused on the variability related to the Indian summer monsoon. It is yet to be determined to what extent the coupled air–sea interactions and feedbacks are essential for capturing precipitation variability throughout the seasonal cycle.

Mechanisms controlling precipitation variability over the Indian Ocean also have implications for prospects for its prediction and its remote influence via teleconnection. Kumar et al. (2010) analyzed evolution of precipitation skill based on retrospective forecasts from the National Centers for Environmental Prediction (NCEP) Climate Forecast System (CFS) and found that skill of monthly-mean precipitation decays quickly over the tropical ocean basins other than the tropical eastern Pacific. The decay of forecast skill of seasonal-mean precipitation and SST is compared in Fig. 1 for the Pacific and the Indian Ocean. It is seen that precipitation skill in the Indian Ocean is not only lower initially but also decays more quickly than that over the Pacific. The average precipitation skill is reduced from 0.50 (0.65) at 0-month lead time to 0.28 (0.52) at 3-month lead time over the tropical Indian (Pacific) Ocean, representing a reduction of 44% versus 20% over the Indian and Pacific Oceans, respectively. Meanwhile, the SST forecast skill, although higher than that of precipitation, also decreases with lead time, with

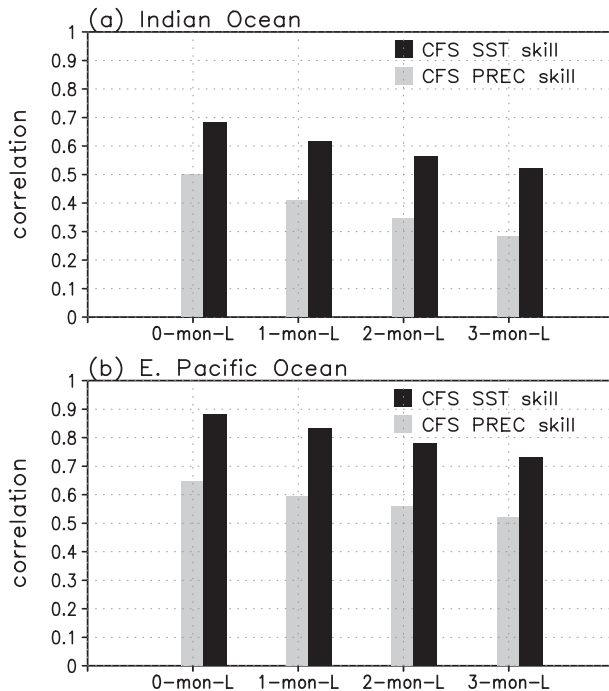


FIG. 1. Area-averaged CFS seasonal-mean forecast correlation skill over (a) the tropical Indian Ocean [20°S–20°N, 30°–120°E] and (b) the tropical eastern Pacific Ocean [20°S–20°N, 180°–300°E] at forecast lead times from 0 to 3 months. The gray bars are for precipitation skill, and the black bars are for the SST skill.

substantially lower skill over the Indian Ocean than that over the Pacific.

Is the lower skill, as well as faster decay, over the Indian Ocean precipitation skill a feature of inherent predictability or is it due to the lower skill for SST prediction over the Indian Ocean (and therefore skill for prediction will improve with improvements in SST forecasts)? One potential avenue to answer this question is the use of the AGCM simulations where observed SSTs are specified. However, AGCM simulations also have a low precipitation skill over the Indian Ocean (Peng et al. 2009; Kumar et al. 2010). It is conceivable that the advantage of having better SSTs in the AGCM simulations is counteracted by lack of coupled air–sea feedback (Kumar and Hoerling 1998; Lau and Nath 2000; van den Dool et al. 2006; Kumar et al. 2007) and, even if SSTs are the same as the observed SSTs, the setup of an AGCM AMIP-type simulation may not provide an accurate estimation for the predictability of precipitation. Therefore, we are still faced with the question that, if the prediction of SST in the Indian Ocean were to improve and if the coupled air–sea feedback is included, will it also lead to improvements in precipitation prediction skill to the levels at par with that over the equatorial eastern Pacific?

These issues are the focus of this study. Specifically, we investigate ocean surface–related factors affecting the precipitation variability over the Indian Ocean that include 1) the influence of remote SST forcing related to ENSO in the tropical Pacific; 2) the role of local SST forcing in the Indian Ocean; and 3) the role of coupled air–sea feedback and the gain in skill due to correct representation of air–sea coupling. Impacts of these factors are analyzed based on a suite of numerical experiments in which SST and coupled air–sea interaction have a varying degree of accuracy. The paper is structured as follows: model simulations and the analysis approach are described in section 2, results are presented in section 3, and a summary and discussion of implications of the analysis for the prediction of seasonal-mean precipitation over tropical Indian Ocean are provided in the closing section 4.

2. Model simulations and analysis approach

Analysis of dynamical predictability and prediction skill of seasonal climate variability is generally based on two modeling approaches. In the first approach, coupled ocean–atmosphere models are integrated from observed initial conditions and SSTs are predicted by the model itself during the course of the integration. For example, the NCEP CFS used for operational seasonal prediction follows this approach. In the second approach, AGCM simulations are performed with the specification of observed SSTs.

Both approaches have their own advantages and disadvantages for the simulation of the atmospheric variability. The first approach includes coupled dynamical and thermodynamical air–sea interaction, but the skill of predicted SSTs is not perfect (Fig. 1). For example, for the CFS skill of SST prediction with lead time beyond 3 months is largely confined to the tropical central and eastern Pacific Ocean (Jin and Kinter 2009; Wang et al. 2010; Kumar et al. 2010). Apart from the correct simulation of the variability, coupled models also have biases in predicted SSTs that may result in erroneous atmospheric variability.

In the second approach of AGCM simulations with the specification of observed SST, although the SST are perfect, coupled air–sea interaction is not included, which may degrade the response of the atmosphere to the specified SSTs. To address the issues raised in the introduction, we analyze four different model simulations that to a varying degree of realism include the observed evolution of SST and coupled air–sea interaction and are based on a design of model simulations that fall in between two modeling approaches outlined above.

a. The model

The simulations used in this study are based on the NCEP operational CFS model. The CFS is a fully coupled ocean–land–atmosphere dynamical seasonal prediction system. The atmospheric component of the CFS is the 2003 version of the NCEP atmospheric Global Forecast System (GFS) model with a spectral truncation of 62 waves (T62) in the horizontal (which is equivalent to nearly a 200-km grid) and a finite differencing in the vertical with 64 sigma layers. The oceanic component of the CFS is the Geophysical Fluid Dynamics Laboratory Modular Ocean Model version 3 (MOM3; Pacanowski and Griffies 1998). The domain is quasi global, extending from 74°S to 64°N with a zonal resolution of 1° and a meridional resolution of $\frac{1}{3}^\circ$ between 10°S and 10°N, gradually increasing through the tropics until becoming fixed at 1° poleward of 30°S and 30°N. There are 40 layers in the vertical with a vertical resolution of 10 m from the surface to the 240-m depth, gradually increasing to about 511 m in the bottom layer around 4.5-km depth. The atmospheric and oceanic components are coupled without any flux adjustment. The two components (i.e., ocean and atmosphere) exchange daily averaged quantities once a day. A more detailed description of the model and analysis of its performance based on the hindcast and free runs can be found in W. Wang et al. (2005) and Saha et al. (2006).

b. Model simulations

We analyze four types of ensemble simulations with the CFS. All simulations are for January 1996–December 2008, and each simulation consists of an ensemble of nine runs started from differing atmospheric initial conditions. Differences in the specification of observed SST and the inclusion of coupled air–sea interaction among the simulations are summarized in Table 1 and further details are as follows:

1) The global SST relaxation (GSSTR) simulation: This simulation is carried out with the coupled CFS. To constrain the SST to the evolution of the observed SST, a relaxation approach is used. This is achieved by a restoring term that relaxes the model's predicted SST toward the observed SST with an e -folding time scale of 3.3 days. The relaxation is computed once per day using observed monthly-mean SSTs that are linearly interpolated to each day. The resulting SST is close to that observed, whereas the coupled air–sea interaction included in the model also has some influence on the SST evolution. In this simulation, the source of the ensemble-mean precipitation variability (i.e., the variability that is common to all members in the ensemble) over the Indian Ocean

TABLE 1. A summary of four simulations GSSTR, PSSTR, GOGA, and POGA in terms of the local SST forcing in the Indian Ocean, the remote ENSO-related SST forcing in the tropical eastern Pacific Ocean, and the extent coupled air–sea interaction is maintained in the Indian Ocean.

Model simulations	Local SST forcing	ENSO SST forcing	Air–sea coupling
GSSTR	near observed (3.3-day SST relaxation)	near observed (3.3-day SST relaxation)	partial (3.3-day SST relaxation)
PSSTR	predicted	observed	yes
GOGA	observed	observed	no
POGA	observed climatology	observed	no

includes (i) dynamical response to remote SST forcing via atmospheric circulation, (ii) interannual variability in local SST, and (iii) interannual variability in local SST that itself is due to remote SST forcing.

2) The Pacific SST relaxation (PSSTR) simulation: This simulation also uses a restoring term for SST but only for the tropical Pacific Ocean. Within the equatorial tropical Pacific region (10°S–10°N, 140°–285°E), the restoring time scale is 3.3 days as in the GSSTR. In the transition zones of 10° latitude/longitude around this region, the restoring time scale increases linearly from 3.3 days at the inner boundary of the transition zones to infinity at the outer boundary of the transition zones. Therefore, outside of tropical Pacific Ocean, there is no direct information of local observed SSTs, the atmosphere and ocean are fully coupled, and SSTs are free to evolve. Over the Indian Ocean, the ensemble-mean SST variability in this simulation is due to the response to remote SST forcing communicated via the atmospheric circulation and possibly due to local air–sea coupling. We note that although the SST variability due to coupled air–sea interaction over the tropical Indian Ocean also has influence on the ENSO variation (e.g., Luo et al. 2010), this aspect is not the focus of this study. Figure 2 shows the temporal correlation of ensemble-mean seasonal-mean SST simulated in PSSTR with the observations from 1996 to 2008 over the tropical Indian and Pacific Oceans. The correlation skill is generally higher than 0.8 in the tropical western Pacific and higher than 0.9 in the tropical central to eastern Pacific because of the restoring of the observed SST over this region. Over a large part of the Indian Ocean, the correlation is 0.5 or higher (e.g., around 10°N in the Arabian Sea and to the northeast of Madagascar), whereas the SST skill is relatively low in the northern part of Bay of Bengal, near the

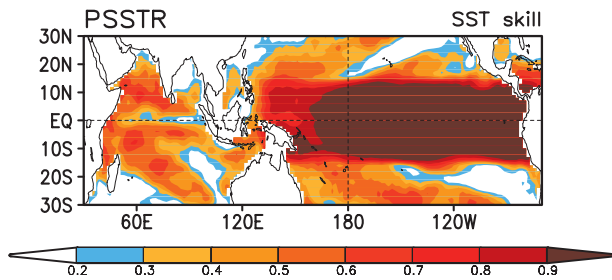


FIG. 2. The spatial distribution of correlation skill for seasonal-mean SST over the tropical Indian and Pacific Oceans from the PSSTR simulation. The shading starts from 0.2, with 0.1 intervals.

equator, and to the southeast of Cocos Island (around 15°S, 100°E). The sources for the ensemble-mean precipitation variability over the Indian Ocean in this simulation primarily include (i) the remote impact from the ENSO-related SST in the tropical eastern Pacific through atmospheric teleconnection and (ii) local influence from the SSTs that are driven by the remote SST anomalies in the tropical Pacific, which can be thought as an indirect influence of ENSO SST on the precipitation variability over the Indian Ocean.

- 3) The global ocean forced global atmospheric (GOGA) simulation: This simulation is an AMIP-type integration with the GFS, the atmospheric component of the CFS. The simulation is forced by observed SSTs over the globe. The SST is updated once per day using observed monthly-mean SSTs that are linearly interpolated to each day. Therefore, the sources of the ensemble-mean precipitation variability in the Indian Ocean are same as for the GSSTR simulation; however, coupled air–sea interaction is not included.
- 4) The Pacific Ocean forced global atmospheric (POGA) simulation: This simulation is the same as the GOGA simulation, except that the observed monthly-mean SST is specified only over the tropical Pacific Ocean (10°S–10°N, 140°–285°E) and the seasonal cycle of the climatological monthly-mean SST is specified in the other ocean basins. Thus, the source of the ensemble-mean precipitation variability over the Indian Ocean is only from the remote forcing related to ENSO SST.

We should point out that for the GSSTR and PSSTR simulations a relaxation time of zero (infinity) is equivalent to the AMIP-type AGCM (fully coupled) simulation. For the former, SST is constrained to evolve as the observed SST and the feedback due to coupled air–sea interaction is not included. For the latter, although SST is no longer constrained to be the same as the observed, a consistent coupled air–sea feedback is included.

c. Analysis

Different treatments of ocean surface in four simulations allow for an analysis of the influence of different factors on the precipitation variability over the Indian Ocean. For example, in the POGA simulation the ensemble-mean precipitation variability is solely from the remote ENSO SST forcing. A comparison between PSSTR and POGA provides a further assessment of the influence of SST variability in the Indian Ocean in response to remote ENSO-related SST variability. A comparison between GOGA and POGA allows an examination of the role of accurate SST “predictions” outside the tropical Pacific but in the absence of coupled air–sea interaction. A comparison between the GOGA and the GSSTR simulation is useful in quantifying the role of coupled air–sea interaction in addition to the accurate SST predictions. A comparison between the GSSTR and the PSSTR simulation gives an estimate of the influence SST on precipitation variability when SST is closer to the observed while at the same time a certain degree of coupled air–sea interaction is also included.

The analysis of precipitation variability follows two complementary approaches. In the first approach, the correlations of the ensemble-mean precipitation variability with the observed precipitation variability are analyzed. This analysis therefore assesses the fidelity of interannual precipitation variability against the observed precipitation. In the second approach, local correlations between SST and precipitation are analyzed and the sign of correlation provides information whether SST is a forcing for the atmosphere (i.e., regions of positive correlation) or is forced by the atmosphere (i.e., regions of negative correlation). In addition, some specific aspects related to the understanding of precipitation skill in the Indian Ocean are also analyzed. In particular, we explore the seasonality in skill, the influence of remote SST variability associated with ENSO in the tropical eastern Pacific via the atmospheric bridge mechanism, and the influence of SST related to the Indian Ocean dipole mode (IODM).

In our analysis, the precipitation skill is defined as the temporal correlation between the seasonal anomalies of the model ensemble mean and corresponding observed anomaly. The seasonal anomalies are obtained from a 3-month running mean of monthly anomalies from 1996 to 2008. The observed monthly SST dataset used as the oceanic forcing in the four simulations, and as the verification to evaluate the simulation skill is from the analysis of Reynolds et al. (2002). The observed monthly precipitation is from the Climate Prediction Center (CPC) Climate Anomaly Monitoring

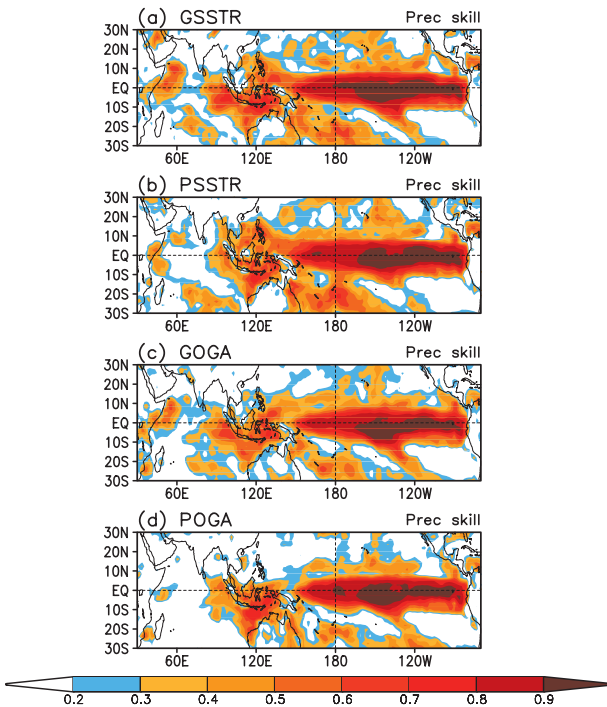


FIG. 3. The spatial distribution of correlation skill for seasonal-mean precipitation from the simulations of (a) GSSTR, (b) PSSTR, (c) GOGA, and (d) POGA. The shading starts from 0.2, with 0.1 intervals.

System–outgoing longwave radiation precipitation index (CAM5–OPI) (Janowiak and Xie 1999).

3. Results

a. General features of precipitation skill

Figure 3 shows the spatial maps of correlation skill for the seasonal-mean precipitation from all four simulations. Their corresponding areal-averaged values over the tropical Indian Ocean and eastern Pacific Ocean are shown in Fig. 4. The skill is calculated based on the entire time series from 1996 to 2008.

As expected, all simulations have the highest precipitation skill in the tropical eastern Pacific where the interannual variability of SST associated with ENSO is the largest. All four simulations show precipitation skill higher than 0.7 over the far equatorial eastern Pacific where the SST forcing is either prescribed or is relaxed to the observed SST. The area-averaged skill over the tropical Pacific for all simulations is above 0.6 (Fig. 4). The difference in skill between forced simulations (i.e., GOGA and POGA) and the SST relaxation simulations (i.e., GRSST and PRSST) is small and, given a short verification time series, not statistically significant. A large precipitation skill resulting from the specification of SSTs is consistent with earlier results in that the

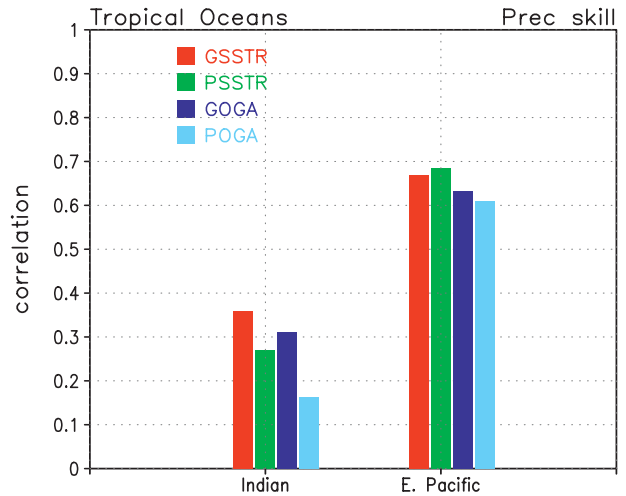


FIG. 4. Area-averaged correlation skill for seasonal-mean precipitation over the tropical Indian Ocean [20°S–20°N, 30°–120°E] and eastern Pacific Ocean [20°S–20°N, 180°–300°E] from the simulations of GSSTR (red bars), PSSTR (green bars), GOGA (blue bars), and POGA (light blue bars).

precipitation over this region is mainly controlled by the interannual SST variability and precipitation variability is slaved to the ocean.

Over the tropical Indian Ocean, the precipitation skill from the four simulations is lower than over the eastern Pacific. This contrast is similar to that for the fully coupled CFS predictions in Fig. 1 and indicates that reasons for low prediction skill in the CFS may not be due to the lack of skill in SST prediction over the Indian Ocean and may be due to inherent predictability limits.

We first discuss the skill in the POGA simulation, which is simplest in terms of SST variability over the Indian Ocean in that it only includes the climatological seasonal cycle. The only region with discernible precipitation skill in POGA simulation is in the vicinity of the eastern edge of Indian Ocean near the coast of Sumatra and Java (Fig. 3d). Because of the design of POGA simulation, this skill is due to the remote influence of SST variability in the equatorial eastern tropical Pacific and is consistent with the documented influence of ENSO over this region (Klein et al. 1999; Lau and Nath 2000, 2003).

Compared to POGA, Indian Ocean SST variability in the PSSTR simulation has an interannual signal that is forced by the remote teleconnection associated with the tropical Pacific SST via the atmospheric bridge (for the skill of SST prediction in the PSSTR, see Fig. 2). This additional SST variability in the Indian Ocean does improve precipitation skill over that for the POGA and can be thought of as the secondary (or indirect) influence of remote ENSO SSTs. The skill of SST prediction for the PSSTR, however, is far from perfect, with correlations generally around 0.5 (Fig. 2). What would be

improvement in precipitation skill if SST followed the observed evolution (i.e., skill of SST prediction is improved)?

For the GOGA simulation (Fig. 3c), the observed SST variability over the Indian Ocean is specified; however, coupled air–sea interaction, as well as feedback, is not included. Nonetheless, specification of correct SST does add incrementally to the skill over that in the POGA and the PSSTR, particularly over the western edge of the Indian Ocean to the coast of Somalia and the mid-southern Indian Ocean. However, even with the specification of correct SST, the level of skill for precipitation over the Indian Ocean is nowhere near that over the equatorial Pacific and leads us back to the question whether this is due to a lack of inherent predictability in precipitation or the lack of coupled air–sea interaction in the design of GOGA simulation.

Possible contribution of coupled air–sea interaction, with SST being close to the observations, and its influence on prediction skill can be gleaned from the GSSTR simulation, which relative to the GOGA simulation also includes a partial representation of the coupled air–sea interaction. In section 3c, from the analysis of local SST–precipitation correlation, we will demonstrate that the GSSTR simulation, as a consequence of coupled air–sea interaction, indeed has a more realistic simulation of the local SST–precipitation relationship. Prediction skill for the GSSTR, in turn, also has an incremental improvement in skill over the GOGA but is still much less than that over the equatorial Pacific.

Going beyond the GSSTR, a complete representation of the coupled air–sea interaction would be similar to the initialized CFS predictions, for which, however, SST trajectory, either because of the inherent predictability limits for SST or because of prediction errors due to model biases, cannot be constrained to be the same as for the observed. Skill of precipitation, even for the CFS predictions with 1-month (2-month) lead time when the influence of the observed initial conditions on the skill has waned (Chen et al. 2010; Kumar et al. 2011), is 0.4 (0.35) (see Fig. 1) and is comparable to the skill for the GSSTR and GOGA simulations.

The progression of precipitation skill from POGA to GSSTR indicates that both the accuracy of SST and the inclusion of coupled air–sea interaction are important for precipitation prediction. However, even with the coupled air–sea interaction and relatively accurate SSTs, for example, in the GSSTR, the absolute precipitation skill over the Indian Ocean is not at par with that over the tropical Pacific. These results suggest that the relatively lower CFS precipitation skill over the Indian Ocean compared to that over the eastern Pacific Ocean is likely because of the inherent predictability limit resulting from a weaker

control of the SST on the precipitation variability over the Indian Ocean and not because of lower skill in SST prediction itself.

b. Seasonality of precipitation skill

Seasonality in precipitation skill is discussed next. Figure 5 shows the spatial maps of seasonal-mean precipitation prediction skill from the four simulations for December–February (DJF), March–May (MAM), June–August (JJA), and September–November (SON), and Fig. 6 shows the area average of skill over the Indian Ocean. Each panel in Fig. 5 is the skill for three running seasons. For example, the maps labeled with DJF are the average of skill for November–January, December–February, and January–March seasonal means.

It is apparent from Fig. 6 that the skill has a distinct seasonality and is largest (smallest) for boreal fall/winter (boreal spring/summer). Further, during fall and winter there are appreciable differences in skill between POGA compared to the GOGA and GSSTR simulations, indicating the importance of having correct interannual SST variability. There is also a small but consistent improvement in skill for the GSSTR relative to the GOGA. The role of interannual variability in SST for improving precipitation skill is further supported by the PSSTR simulation for which skill is generally higher than for POGA. The spatial pattern of precipitation skill for different seasons is discussed next.

For DJF (Fig. 5, left), precipitation skill in the POGA simulation is due to the remote influence of ENSO and is confined to the eastern Indian Ocean. The addition of local SST variability in the Indian Ocean due to ENSO, as well as its feedback on the atmosphere, does lead to a substantial improvement in skill in the PSSTR simulation. Specification of SSTs in the GOGA simulation improves skill in the equatorial Indian Ocean, particularly in the west, and additional improvement in skill occur when the coupled air–sea interaction is also included (i.e., the GSSTR simulation).

For MAM (Fig. 5, second column), precipitation skill is generally lower. Regions with the largest skill are located in the Bay of Bengal and southwestern tropical Indian Ocean. In the Southern Hemisphere, precipitation skill is likely to be associated with the asymmetric mode of tropical Indian Ocean precipitation variability. Previous studies have shown that the spring asymmetric precipitation mode is closely related to air–sea interactions in the tropical Indian Ocean and to the remote influence from ENSO and is better simulated when the air–sea coupling is included in the Indian Ocean (Wu and Kirtman 2004; Wu et al. 2008; Wu and Yeh 2010). Our results are consistent with the results from these

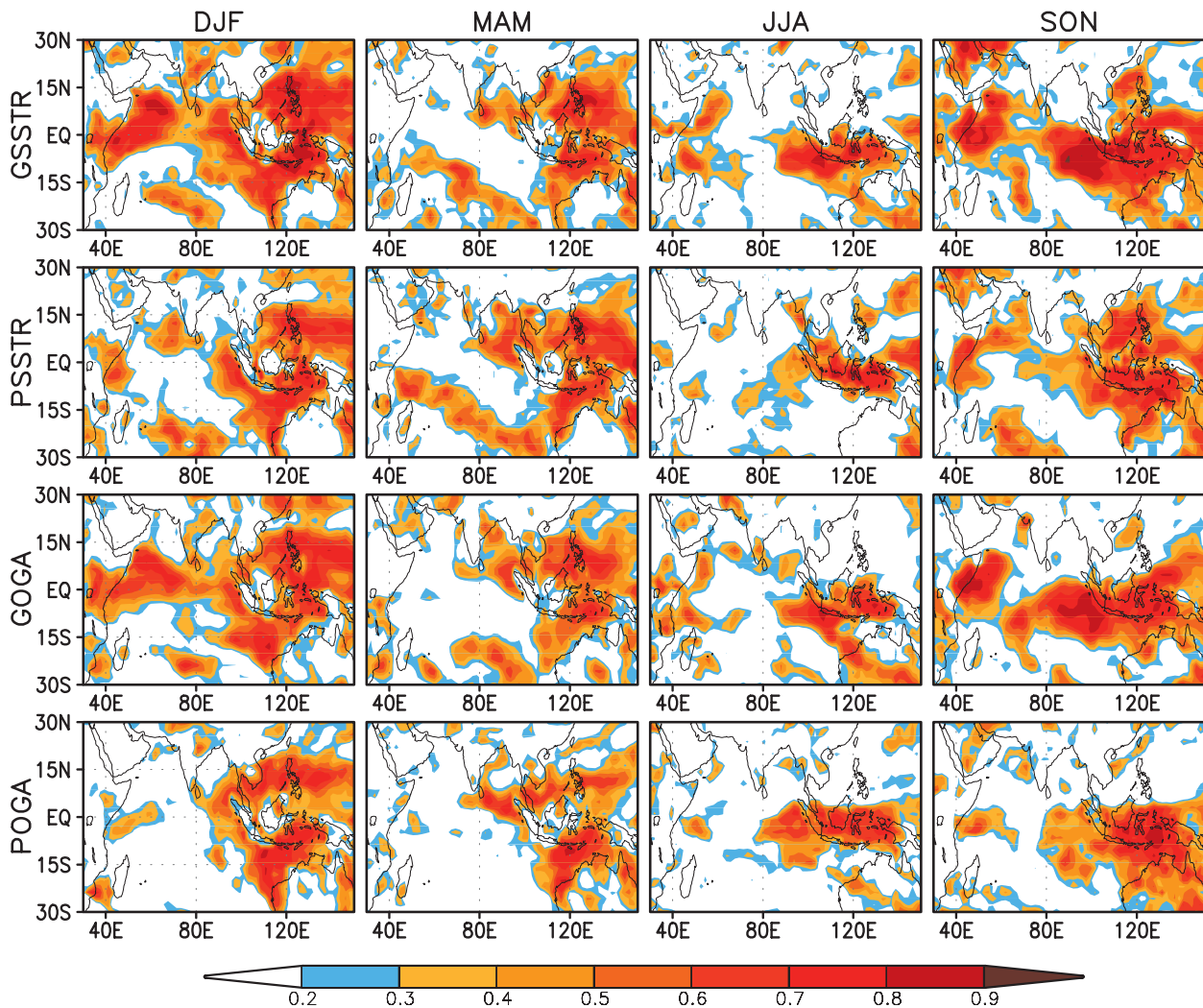


FIG. 5. Spatial distribution of correlation skill for seasonal-mean precipitation over the region of the tropical Indian Ocean from the simulations of (top)–(bottom) GSSTR, PSSTR, GOGA, and POGA in the seasons (left)–(right) DJF, MAM, JJA, and SON. The shading starts from 0.2, with 0.1 intervals.

previous studies and show that during MAM the atmospheric variability in the Indian Ocean is better captured with the full air–sea coupling as is the case for PSSTR than with partial coupling and reasonable SSTs (as for GSSTR) or with perfect SSTs but no coupling (as in GOGA).

During JJA (Fig. 5, third column), all four simulations show relatively low prediction skill for seasonal-mean precipitation over the Indian Ocean, and neither the use of observed SSTs (GOGA) nor the inclusion of full coupling (PSSTR) leads to improvement in skill over the Indian Ocean. The highest skill in the Indian Ocean is confined to the region off Sumatra and is associated with ENSO forcing as is already evident in the POGA simulation. Low precipitation skill during JJA may be due to the fact that the interannual variability of SST during

this season is the lowest (Fig. 7, bottom), leading to a low inherent signal that can be predicted. Another possibility is that the summertime rainfall may be associated with subscale convective events and may be more difficult to predict at longer leads (Wang et al. 2004). It is also noted that on average the skill in POGA is slightly better than that in PSSTR in this season (Fig. 6). The reason for this is not clear. One possibility is that the SST bias in the PSSTR adversely degrades the model's performance in this season, or the difference is not statistically significant because of a short verification time series.

For SON (Fig. 5, right), precipitation skill is highest of all four seasons (also see Fig. 6). The skill in GSSTR and GOGA are much higher than the other two simulations, indicating that SST accuracy during this season is

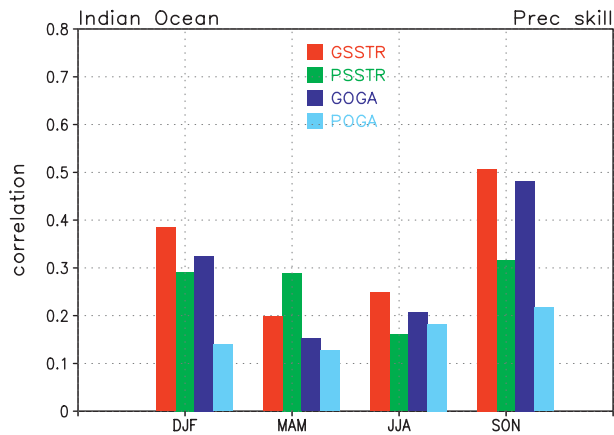


FIG. 6. Area-averaged correlation skill for seasonal-mean precipitation over the tropical Indian Ocean [20°S–20°N, 30°–120°E] from the simulations GSSTR (red bars), PSSTR (green bars), GOGA (blue bars), and POGA (light blue bars) in the seasons DJF, MAM, JJA, and SON.

beneficial for the simulation of precipitation variability in the Indian Ocean. As will be discussed in section 3d, the higher precipitation skill is related to the atmospheric response to the IODM. The IODM, featuring an east–west contrast of SST anomalies (Saji et al. 1999; Webster et al. 1999), develops in summer and peaks in fall.

The analysis of seasonal variability of skill can be summarized as follows: precipitation skill is largest for SON and smallest for JJA; for SON, there is large improvement in skill from the specification of SST variability; and the inclusion of coupled air–sea interaction does help improve prediction skill but is not a crucial factor, and this is true for all the seasons but MAM. The peculiar behavior of the PSSTR for MAM will be discussed further in section 3e.

c. Local precipitation–SST relationship

A key aspect in understanding the predictability of seasonal-mean precipitation is the relationship between SST and precipitation: that is, is the slowly varying SST variability responsible for precipitation variability (as is the case for tropical eastern Pacific) or is it a consequence of atmospheric variability itself? For the former (latter), one would expect a positive (negative) precipitation–SST correlation. For the predictability of precipitation, a slower time scale associated with the SST forcing may also be associated with higher predictability for precipitation. Further, if SST forcing for the atmosphere dominates, atmospheric model simulations alone are likely able to capture the predictable component when forced by the observed SST. On the other hand, if the observed SST anomalies are a result of atmospheric variability, which itself is unpredictable beyond the weather time scale, AGCMs with specified SST forcing will have difficulty in

reproducing observed precipitation variability (B. Wang et al. 2004, 2005; Wu and Kirtman 2005). An assessment of the precipitation–SST relationship therefore helps discern the role of SST on precipitation variability and may also help clarify the regional dependence of skill in four simulations.

Figure 7 shows the spatial distribution of the local simultaneous correlation between seasonal anomalies of precipitation and SST from observations (top row) and simulations of GSSTR (second row) and GOGA (third row). Similar to Fig. 5, the correlations are shown for four seasons: DJF, MAM, JJA, and SON. For the POGA simulation, the precipitation–SST correlation cannot be computed because of a lack of interannual SST variability. For the PSSTR simulation, in which the SST variability over the Indian Ocean is internal to the model, although the precipitation–SST relationship is self-consistent (as is for observations), because of error in the simulation of SST variability the spatial structure of correlation is not directly comparable with the observations. Thus, the precipitation–SST correlations from POGA and PSSTR are not included in the analysis. Further, we calculate the precipitation–SST correlation for each individual simulation and then average the correlation from all simulations. To further understand the role of SST, the standard deviation of SST seasonal anomaly for different seasons is also shown in Fig. 7 (bottom).

As shown in Fig. 7, the precipitation–SST correlation displays considerable geographical and seasonal variation. For observations, the highest positive correlations are generally collocated with regions having the largest interannual variability in SST. DJF shows high positive correlations over the western tropical Indian Ocean near the coast of Somalia and the southwest Indian Ocean. In MAM, SST variability is relatively weak, and positive correlations are mainly confined to the southwestern Indian Ocean and negative correlations extend from the northeastern Indian Ocean to the coast of Sumatra. Associated with a large SST variability related to the IODM, which develops in JJA and peaks in SON (Fig. 7, bottom), the weak negative correlation in MAM changes to a strong positive correlation over the west coast of Sumatra in JJA and SON. The positive correlations over the eastern and western tropical Indian Ocean are also enhanced in SON. Observed precipitation–SST correlations also have regions with negative values. It is also worth noting that (i) positive correlation is not as strong as over the tropical eastern Pacific (not shown), indicating less control by the SST, and (ii) over a large area of the Indian Ocean correlation is near zero, implying a lack of consistent relationship between SST and precipitation variability on seasonal time scale.

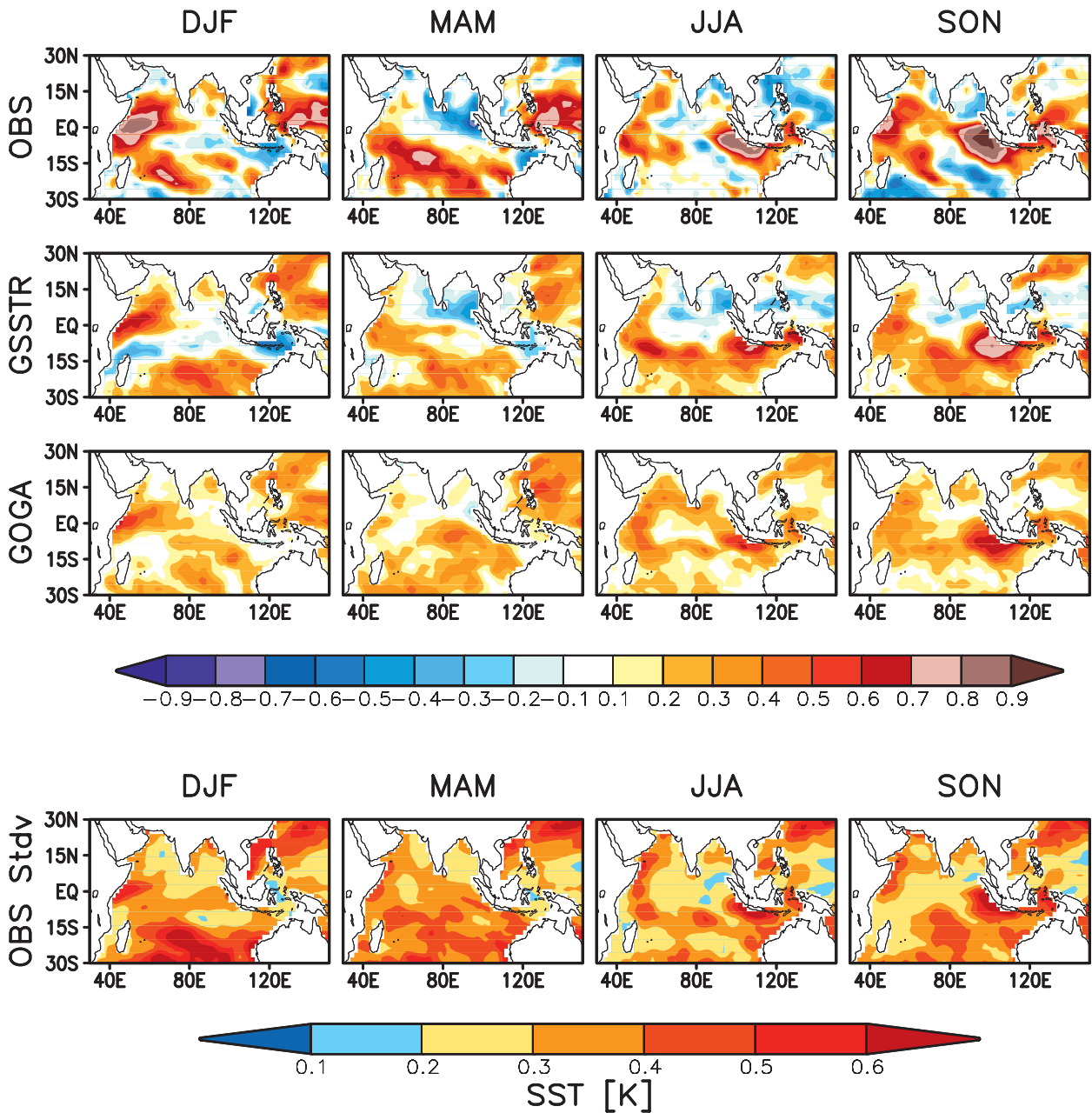


FIG. 7. The spatial distribution of simultaneous temporal correlation between seasonal-mean precipitation and underlying SST from (top) observations, (top middle) the GSSTR simulation, and (bottom middle) the GOGA simulation in the seasons (left)–(right) DJF, MAM, JJA, and SON. The correlation shading interval is 0.1. (bottom) The corresponding observed SST standard deviation in the four seasons. The SST units: kelvins (K), and the shading interval is 0.1 K.

To a large extent, the GSSTR simulation (which includes air–sea interaction and a SST relaxation with the time scale of 3.3 days) replicates the seasonal cycle of the precipitation–SST correlation pattern seen in observations. The GSSTR simulation also replicates the regions of negative SST correlation, whereas, because of the specification of SST, the GOGA correlations everywhere are positive. Therefore, although the SST in the GSSTR is

relaxed to the observed value, it still allows for a negative SST–precipitation correlation. For the GOGA, the lack of a negative SST–precipitation correlation is a common deficiency noted in simulations with specified SST in AGCMs (Trenberth and Shea 2005; B. Wang et al. 2004, 2005; Wu et al. 2006). The regions of a strong positive precipitation–SST correlation for the GOGA generally coincide with that for the GSSTR.

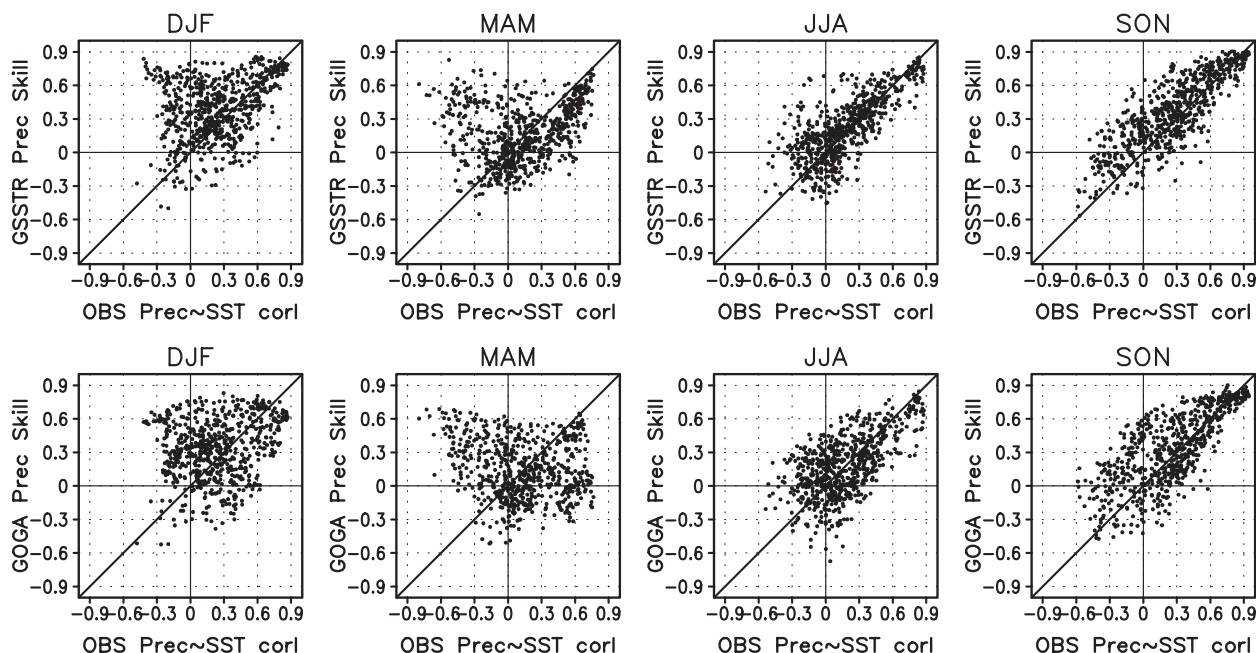


FIG. 8. Scatterplot between the precipitation skill in simulations (the y axis) and the observed precipitation–SST correlation (the x axis) over the Indian Ocean region [20°S–20°N, 30°–120°E] from the seasons of DJF, MAM, JJA, and SON: for (top) GSSTR and (bottom) GOGA.

We next discuss the relationship between the precipitation–SST correlation and the precipitation skill. As summarized earlier, a positive precipitation–SST correlation implies a forcing for the atmospheric variability by the underlying SSTs. Another implication is that correct evolution (e.g., when specified) of SST in model simulations (e.g., GSSTR and GOGA) should also lead to a skillful precipitation forecast. This is generally true as can be gleaned from the comparison of areas of positive correlation in Fig. 7 (top, for observations) and areas with positive skill for precipitation (Fig. 5).

A better visualization of this relationship is via a scatterplot between precipitation skill and the observed precipitation–SST correlation shown in Fig. 8. For a positive precipitation–SST correlation, in general, there is a quasi-linear relationship with the precipitation skill, and this generally holds true for all seasons, except MAM in GOGA. In other words, over the regions of positive precipitation–SST correlation, potential predictability of seasonal-mean precipitation is high. Actual prediction, however, would require a skillful prediction of SSTs. It is also interesting to note that the amplitude of positive precipitation–SST correlations is much larger than their negative counterparts. This is to be expected because slowly varying SST (particularly if a consequence of ocean dynamics) acting as a forcing for the atmosphere can lead to a large positive precipitation–SST correlation (as is the case for the equatorial Pacific). On the other

hand, persistent precipitation anomalies as a consequence of atmospheric circulation are generally not long lived and cannot lead to substantial SST cooling (due to a reduction in surface shortwave flux and other feedbacks) on a seasonal time scale.

Precipitation skill over the regions of negative precipitation–SST correlation falls under two regimes. The first regime is the regions where precipitation–SST correlation is negative but the precipitation skill is positive. These regions are the points that populate the top-left quadrant in Fig. 8 and are more frequent in DJF and MAM. A specific example is the area of negative precipitation–SST correlation in MAM in the eastern Indian Ocean north of the equator between Sri Lanka and northern Sumatra (Fig. 7) over which precipitation skill is positive. A likely explanation is that precipitation over these regions is forced remotely by the tropical Pacific SST and in turn leads to a reduction in SST. The former link provides positive skill for precipitation due to remote forcing, whereas the latter provides a negative precipitation–SST correlation. Supporting evidence for this causal link is further provided by the precipitation skill for the POGA simulation (Fig. 5, bottom, for DJF and MAM) that also has positive precipitation skill in response to ENSO SST even when no SST variability in the Indian Ocean is specified.

The other regime of negative precipitation–SST correlation occurs when seasonal-mean precipitation anomalies generate cooling in the underlying SSTs and the

associated atmospheric circulation itself results from internal atmospheric dynamics and is unpredictable on a seasonal time scale. One would expect that precipitation skill for such instances to be small. This is the case for region over the southern Indian Ocean for SON, where precipitation skill for the GSSTR and the GOGA simulation is small and at the same time the observed precipitation–SST correlation is negative.

In summary, spatial features in precipitation skill are generally consistent with the spatial distribution of precipitation–SST correlation with areas of positive correlation (i.e., forcing of the atmosphere by SST) having (a large) positive precipitation skill and areas of negative precipitation–SST correlation, except for the places where precipitation is forced remotely because of ENSO SST, having small precipitation skill. The results once again suggest that low precipitation skill over the Indian Ocean therefore may be an inherent feature of climate variability over the Indian Ocean.

d. Prediction skill from IODM

The analysis of the precipitation–SST relationship shows a strong positive correlation over the western coast of Sumatra in JJA and SON. It is also well known that a substantial portion of the interannual SST variability over this region is associated with the IODM events (e.g., Saji et al. 1999; Webster et al. 1999). The key characteristic of the IODM is the reversal in sign of SST anomalies across the basin between the region off Sumatra and the western Indian Ocean basin. Typically, the IODM develops around June, intensifies in the following months, and peaks in October. As reported in early studies (e.g., Luo et al. 2007, 2008, 2010; Saji et al. 2005), the IODM shows significant influence on precipitation and temperature variability over the Indian Ocean and surrounding region and remotely on ENSO over the eastern Pacific. As shown in Fig. 7, there is a strong positive correlation between precipitation and SST over both the eastern and the western nodes of the IODM that indicates SST acts as a forcing for the atmosphere. In this section, we further analyze the influence of the IODM-related SST variability on precipitation. With the anticipation that the SST is forcing for the atmospheric variability, results for the GSSTR and GOGA simulations alone are shown.

Shown in Fig. 9 are the GSSTR and GOGA precipitation skill over the tropical Indian Ocean and the observed normalized SST Indian Ocean dipole mode index (IODMI) from 1996 to 2008. The IODMI is defined as the difference in SST anomaly between the tropical western Indian Ocean (10°S – 10°N , 50° – 70°E) and the tropical southeastern Indian Ocean (10°S – 0° , 90° – 110°E). During the analysis period, there are four strong IODM events for which the IODMI exceeds 1.5 of its standard

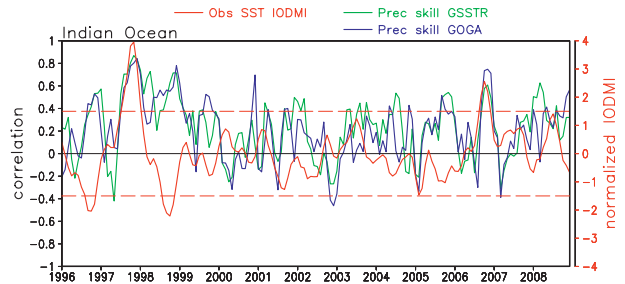


FIG. 9. The time series of seasonal-mean precipitation correlation skill averaged over the tropical Indian Ocean [20°S – 20°N , 30° – 120°E] from the simulations of GSSTR (green line) and GOGA (blue line) and the normalized IODMI from observations (red line).

deviation. These events are for SON of 1996, 1997, 1998, and 2006. From the time series of precipitation skill, it is also apparent that for both GSSTR and GOGA precipitation skill is high during the IODM events (Fig. 9, blue and green curves).

Figure 10 shows composite maps of the observed SST, the observed precipitation, the simulated precipitation from GSSTR and GOGA for the above four IODM events. The composite maps are the average of two positive IODM events (SON 1997 and SON 2006) minus the average of two negative IODM events (SON 1996 and SON 1998). From the spatial pattern of the SST anomaly, it is clear that associated with the IODM events there is sharp SST gradient between the eastern and western tropical Indian Ocean with the cold SST anomalies over the eastern side off Java–Sumatra and warm SST anomalies over the western side off Somalia and the southwestern Indian Ocean.

Corresponding to the anomalous SST, the observed precipitation is reduced over the eastern equatorial Indian Ocean throughout Indonesia while it is increased over the western equatorial Indian Ocean and parts of Africa. The sign of precipitation anomaly is such that enhanced (reduced) precipitation is generally collocated with the positive (negative) SST anomaly, consistent with positive precipitation–SST correlation for this season. The GOGA simulation reproduces well the observed precipitation variation for the IODM events and confirms that the variations in SST are responsible for the precipitation variability. Similar precipitation anomalies are also replicated in the GSSTR simulation. The pattern correlations of composite precipitation between the model simulations and observations are 0.70 for GSSTR and 0.75 for GOGA. The slightly better correlation in GOGA than in GSSTR may suggest that the accurate SST forcing is a dominant factor for the precipitation variability during the extreme IODM events. To summarize, the SST variability associated with the IODM

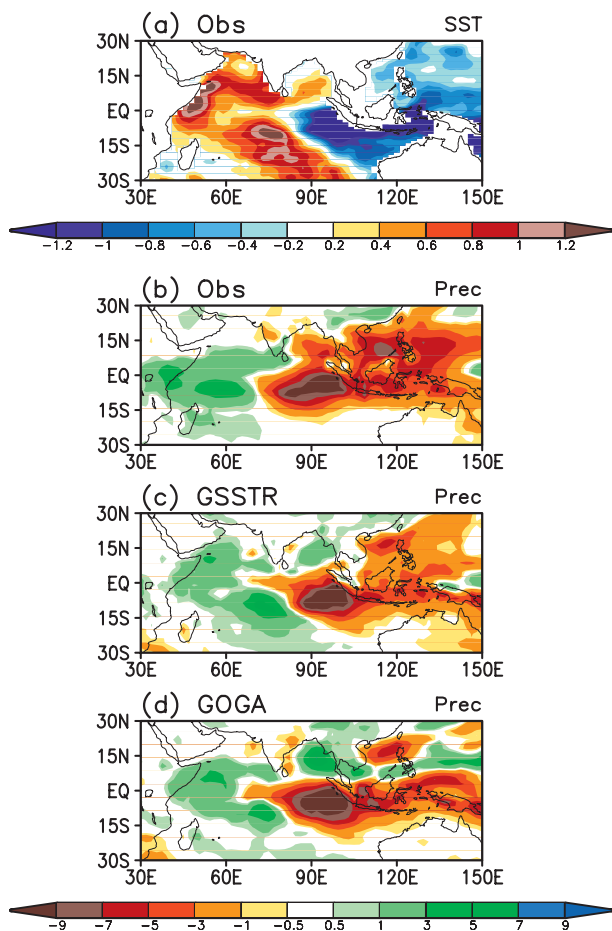


FIG. 10. (a) The composite seasonal anomalies of SST from observations and precipitation from (b) observations, (c) the GSSTR simulation, and (d) the GOGA simulation based on two strong positive IODMI seasons (SON 1997 and SON 2006) and two strong negative IODMI seasons (SON 1996 and SON 1998). Precipitation units: mm day^{-1} and SST units: kelvins.

represents a strong forcing for the atmosphere, acts in a manner similar to the SST variability associated with ENSO in the tropical eastern Pacific, and leads to a high precipitation skill during JJA and SON.

e. Analysis of the ENSO influence

Different configurations for the SST variability in four simulations also allow us to quantify the effect of remote ENSO variability over the Indian Ocean. In the PSSTR simulation, the SST is relaxed to the observed SST over the tropical Pacific Ocean, whereas it is predicted elsewhere. Therefore, the source of Indian Ocean SST variability in that simulation is from the SST variability associated with ENSO in the tropical eastern Pacific Ocean via the atmospheric bridge mechanism, as shown in Fig. 2.

To quantify the influence of ENSO on Indian Ocean SST variability, Fig. 11 shows the time series of the

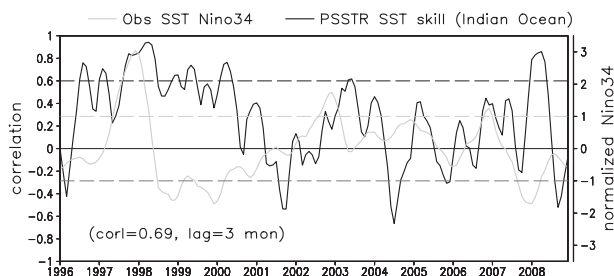


FIG. 11. The time series of seasonal-mean SST correlation skill averaged over the tropical Indian Ocean (20°S – 20°N , 30° – 120°E) from the PSSTR simulation (black curve) and the normalized Niño-3.4 SST from observations (gray curve). The maximum value of the lag correlation between the time series of the SST skill and Niño-3.4 SST and the lag are shown in the bottom-left corner.

normalized Niño-3.4 SST from observations (gray curve) and the SST correlation skill in the PSSTR simulation over the tropical Indian Ocean (black curve). During the time period from 1996 to 2008, the years with higher SST skill is closely related to ENSO events. For example, the SST skill higher than 0.6 in years 1998, 1999, 2000, 2003, 2007, and 2008 are about 3 months after the large amplitudes of Niño-3.4 SST. The maximum correlation between the PSSTR SST skill and the Niño-3.4 SST is 0.69 at a 3-month lag and is consistent with delay of ENSO-related SST anomalies in other tropical ocean basins (Klein et al. 1999; Kumar and Hoerling 2003; Saji et al. 2006).

The influence of ENSO on precipitation variability over the Indian Ocean is analyzed from a comparison of the PSSTR and POGA simulations. We compare the precipitation skill in PSSTR and POGA stratified based on different level of SST prediction skill in the PSSTR simulation. Figure 12 shows the PSSTR and POGA precipitation skill from the months with low PSSTR SST prediction skill (less than 0.6 in Figs. 12a,b) and those with higher PSSTR SST prediction skill (equal to or greater than 0.6 in Figs. 12e,f). In all, there are 32 seasons out of a total of 156 for which PSSTR SST skill is equal to or greater than 0.6 (Fig. 11). When the SST prediction skill is <0.6 , the precipitation skill of the PSSTR and the POGA is similar. For SST skill >0.6 , there is clear improvement in precipitation skill for the PSSTR over the POGA, which implies the secondary influence of ENSO variability in the Indian Ocean is induced via changes in the SST.

To assess if the correct rendition of air–sea interaction in PSSTR leads to a better precipitation prediction skill or if skill is compromised because of errors in SST evolution, we compare the precipitation skill in PSSTR and GOGA. When PSSTR SST skill is high, it shows somewhat better precipitation skill than GOGA in general.

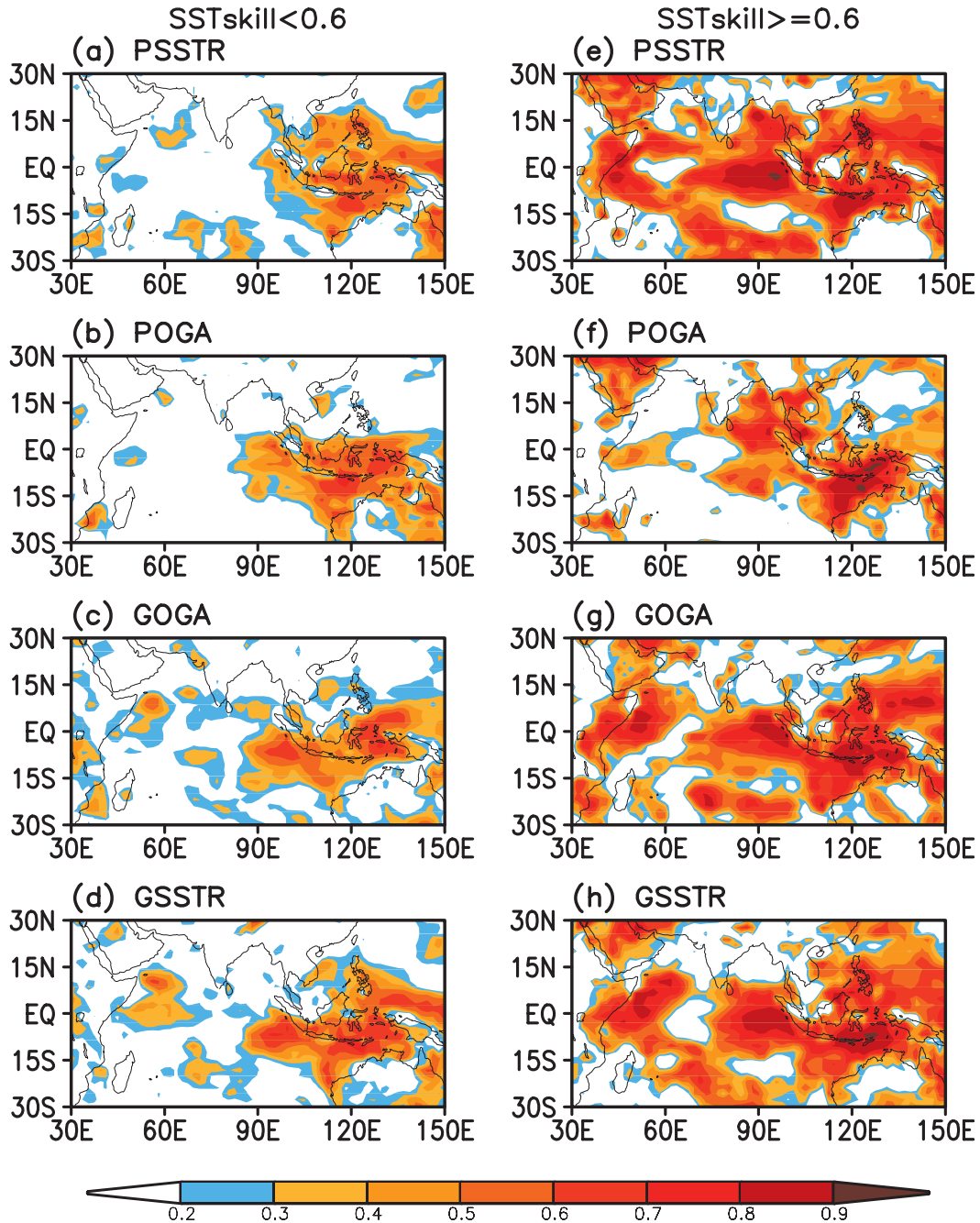


FIG. 12. The spatial distribution of seasonal-mean precipitation correlation skill from the PSSTR, POGA, GOGA, and GSSTR simulations for those months (a)–(d) when the seasonal-mean SST correlation skill in PSSTR is less than 0.6 and (e)–(h) when SST correlation skill is equal to or greater than 0.6. The shading starts from 0.2, with 0.1 intervals.

GOGA misses the precipitation skill over the Bay of Bengal and the southwest part of the Indian Ocean where PSSTR shows high precipitation skill. The average precipitation skill over the tropical Indian Ocean is 0.60 in PSSTR (Fig. 12e) compared to 0.45 in GOGA (Fig. 12g) when the PSSTR SST skill is high. However, GOGA

shows small improvement in skill when the PSSTR SST correlation skill is low: the average precipitation skill is 0.25 in GOGA (Fig. 12c) compared 0.14 in PSSTR (Fig. 12a). These results suggest that the coupled air–sea interaction adds to the precipitation skill when the SST variability is reasonably represented in the Indian Ocean.

For the sake of completeness, precipitation skill for the GSSTR is also shown.

As is apparent from Fig. 11, PSSTR SST correlation skill over tropical Indian Ocean lags Niño-3.4 SST variation by 3 months. Consequently, PSSTR simulates SST variation better in MAM, which is about one season following the peak in ENSO in boreal winter in DJF. Given a better simulation of SST variation in MAM, the coupled air–sea interaction in the Indian Ocean in PSSTR also leads to better precipitation skill in PSSTR than in GOGA and GSSTR MAM (Figs. 5, 6).

4. Summary and conclusions

To understand the prospects of seasonal climate prediction skill over the Indian Ocean and surrounding regions, we have analyzed possible factors affecting the seasonal-mean precipitation variability and its prediction skill. We focus the analyses on the contributions from the local SST forcing in the Indian Ocean, the remote SST forcing related to ENSO in the tropical eastern Pacific Ocean, and the role of air–sea coupling. The analysis is based on four simulations with the NCEP CFS using different treatments of the ocean surface. These simulations are 1) the global SST relaxation (GSSTR) simulation; 2) the Pacific SST relaxation (PSSTR) simulation; 3) the global ocean forced global atmospheric (GOGA) simulation; and 4) the Pacific Ocean forced global atmospheric (POGA) simulation. The seasonal-mean precipitation skills in the tropical Indian Ocean from these four simulations were examined and compared.

In general, GSSTR, PSSTR, and GOGA show better skill than POGA, which indicates the accurate local SST forcing in the Indian Ocean is important in the seasonal precipitation prediction. This is also confirmed by the fact that regions of positive precipitation–SST correlation in observations have the highest precipitation skill (Figs. 5, 7, 8). Inclusion of coupled air–sea feedback in the Indian Ocean does help improve precipitation skill. For example, the PSSTR simulation performs better than the POGA simulation and shows a higher skill than other simulations in MAM (Figs. 5, 6). However, the inclusion of coupled air–sea interaction alone in the PSSTR simulation is not sufficient to bring over the precipitation skill on par with that of the GOGA simulation, and overall the skill of the GOGA simulation is closer to that of the GSSTR simulation than the PSSTR simulation skill (Figs. 3–6). The results therefore indicate that the skill of precipitation in the GOGA simulation is a fair estimate of its potential predictability and is not unduly influenced by the lack of coupled air–sea interactions.

The prediction skill of precipitation, as well as the impacts from the SST forcing and air–sea coupling, also

has a strong seasonal variation. The precipitation prediction skill is much higher in DJF and SON than in MAM and JJA because of stronger ENSO-related SST forcing in these two seasons and also because of the peak phase of the IODM (in SON). In MAM, when the SST variation in the tropical Indian Ocean resulting from the delayed influence from ENSO-related SST forcing in the previous winter is captured well, the simulation with full air–sea coupling in the Indian Ocean (PSSTR) shows better precipitation skill than GSSTR and GOGA, indicating the some importance of air–sea coupling during this particular season.

The current study can be further enhanced in the following two aspects: First, the precipitation skill differences between PSSTR with fully interactive air–sea coupling in the Indian Ocean and the other three simulations either with no air–sea coupling (GOGA and POGA) or with partial air–sea coupling (GSSTR) may also result from the differences in their mean SST states. Therefore, it will be helpful to examine the role of the air–sea coupling by comparing the simulation in a coupled model with that of an AGCM simulation that is forced with the SST generated from the same coupled model. The second is that all four types of simulations used in this study include observed remote ENSO-related SST forcing in the tropical eastern Pacific. Although many previous studies have shown that the remote ENSO-related forcing has strong influence over the Indian Ocean (Nigam and Shen 1993; Klein et al. 1999; Lau and Nath 2000; Annamalai et al. 2005; Wu et al. 2008; Luo et al. 2010; results herein), it would be interesting to have analysis from an additional simulation without ENSO forcing. This might help to identify to what extent the precipitation skill is contributed solely from the local SST forcing in the Indian Ocean. These issues will be investigated in future work and results will be reported accordingly.

Acknowledgments. Constructive comments from Drs. Zeng-Zhen Hu and Scott Weaver and two anonymous reviewers are gratefully acknowledged.

REFERENCES

- Alexander, M. A., I. Bladé, M. Newman, J. R. Lanzante, N.-C. Lau, and J. D. Scott, 2002: The atmospheric bridge: The influence of ENSO teleconnections on air–sea interaction over the global oceans. *J. Climate*, **15**, 2205–2231.
- Annamalai, H., S.-P. Xie, J.-P. McCreary, and R. Murtugudde, 2005: Impact of Indian Ocean sea surface temperature on developing El Niño. *J. Climate*, **18**, 302–319.
- Arakawa, O., and A. Kitoh, 2004: Comparison of local precipitation–SST relationship between the observation and a reanalysis dataset. *Geophys. Res. Lett.*, **31**, L12206, doi:10.1029/2004GL020283.
- Barnett, T. P., K. Arpe, L. Bengtsson, M. Ji, and A. Kumar, 1997: Potential predictability and AMIP implications of midlatitude

- climate variability in two general circulation models. *J. Climate*, **10**, 2321–2329.
- Brankovic, C., T. N. Palmer, and L. Ferranti, 1994: Predictability of seasonal atmospheric variations. *J. Climate*, **7**, 217–237.
- Chen, M., W. Wang, and A. Kumar, 2010: Prediction of monthly-mean temperature: The role of atmospheric and land initial conditions and sea surface temperature. *J. Climate*, **23**, 717–725.
- Janowiak, J. E., and P. Xie, 1999: CAMS–OPI: A global satellite-rain gauge merged product for real-time precipitation monitoring applications. *J. Climate*, **12**, 3335–3342.
- Jin, E. K., and J. L. Kinter III, 2009: Characteristics of tropical Pacific SST predictability in coupled GCM forecasts using the NCEP CFS. *Climate Dyn.*, **32**, 675–691, doi:10.1007/s00382-008-0418-2.
- Kang, I.-S., and Coauthors, 2002: Intercomparison of atmospheric GCM simulated anomalies associated with the 1997/98 El Niño. *J. Climate*, **15**, 2791–2805.
- Klein, S. A., B. J. Sode, and N.-C. Lau, 1999: Remote sea surface temperature variations during ENSO: Evidence for a tropical atmospheric bridge. *J. Climate*, **12**, 917–932.
- Krishna Kumar, K., M. Hoerling, and B. Rajagopalan, 2005: Advancing dynamical prediction of Indian monsoon rainfall. *Geophys. Res. Lett.*, **32**, L08704, doi:10.1029/2004GL021979.
- Kumar, A., and M. P. Hoerling, 1998: Specification of regional sea surface temperatures in atmospheric general circulation model simulations. *J. Geophys. Res.*, **103**, 8901–8907.
- , and —, 2003: The nature and causes for delayed atmospheric response to El Niño. *J. Climate*, **16**, 1391–1403.
- , S. D. Schubert, and M. S. Suarez, 2003: Variability and predictability of 200-mb seasonal mean heights during summer and winter. *J. Geophys. Res.*, **108**, 4169, doi:10.1029/2002JD002728.
- , B. Jha, Q. Zhang, and L. Bounoua, 2007: A new methodology for estimating the unpredictable component of seasonal atmospheric variability. *J. Climate*, **20**, 3888–3901.
- , M. Chen, and W. Wang, 2011: An analysis of prediction skill of monthly mean climate variability. *Climate Dyn.*, **37**, 1119–1131, doi:10.1007/s00382-010-0901-4.
- Lau, N.-C., and M. J. Nath, 2000: Impact of ENSO on the variability of the Asian–Australian monsoons as simulated in GCM experiments. *J. Climate*, **13**, 4287–4309.
- , and —, 2003: Atmosphere–ocean variations in the Indo-Pacific sector during ENSO episodes. *J. Climate*, **16**, 3–20.
- Livezey, R. E., M. Masutani, and M. Ji, 1996: SST-forced seasonal simulation and prediction skill for versions of the NCEP/MRF model. *Bull. Amer. Meteor. Soc.*, **77**, 507–517.
- Luo, J.-J., S. Masson, A. Behera, and T. Yamagata, 2007: Experimental forecast of the Indian Ocean dipole using a coupled OAGCM. *J. Climate*, **20**, 2178–2190.
- , S. Behera, Y. Masumoto, H. Sakuma, and T. Yamagata, 2008: Successful prediction of the consecutive IOD in 2006 and 2007. *Geophys. Res. Lett.*, **35**, L14S02, doi:10.1029/2007GL032793.
- , R. Zhang, S. K. Behera, Y. Masumoto, F.-F. Jin, R. Lukas, and T. Yamagata, 2010: Interaction between El Niño and extreme Indian Ocean dipole. *J. Climate*, **23**, 726–742.
- Nigam, S., and H.-S. Shen, 1993: Structure of oceanic and atmospheric low-frequency variability over the tropical Pacific and Indian Ocean. Part I: COADS observations. *J. Climate*, **6**, 657–676.
- Pacanowski, R. C., and S. M. Griffies, 1998: MOM 3.0 manual. NOAA/Geophysical Fluid Dynamics Laboratory Rep., 668 pp.
- Peng, P., and A. Kumar, 2005: A large ensemble analysis of the influence of tropical SSTs on seasonal atmospheric variability. *J. Climate*, **18**, 1068–1085.
- , —, and W. Wang, 2009: An analysis of seasonal predictability in coupled model forecasts. *Climate Dyn.*, **36**, 637–648, doi:10.1007/s00382-009-0711-8.
- Reynolds, W. R., N. A. Rayner, T. Smith, D. C. Stokes, and W. Wang, 2002: An improved in situ and satellite SST analysis for climate. *J. Climate*, **15**, 1609–1625.
- Saha, S., and Coauthors, 2006: The NCEP Climate Forecast System. *J. Climate*, **19**, 3483–3517.
- Saji, N. H., B. N. Goswami, P. N. Vinayachandran, and T. Yamagata, 1999: A dipole mode in the tropical Indian Ocean. *Nature*, **401**, 360–363.
- , T. Ambrizzi, and S. E. T. Ferraz, 2005: Indian Ocean dipole mode events and austral surface air temperature anomalies. *Dyn. Atmos. Oceans*, **39**, 87–101, doi:10.1016/j.dynatmoce.2004.10.015.
- , S.-P. Xie, T. Yamagata, 2006: Tropical Indian Ocean variability in the IPCC twentieth-century climate simulations. *J. Climate*, **19**, 4397–4417.
- Schubert, S. D., M. J. Suarez, P. J. Pegion, R. D. Koster, and J. T. Bacmeister, 2008: Potential predictability of long-term drought and pluvial conditions in the U.S. Great Plains. *J. Climate*, **21**, 802–816.
- Shukla, J., and J. M. Wallace, 1983: Numerical simulation of the atmospheric response to equatorial sea surface temperature anomalies. *J. Atmos. Sci.*, **40**, 1613–1630.
- Trenberth, K. E., and D. J. Shea, 2005: Relationships between precipitation and surface temperature. *Geophys. Res. Lett.*, **32**, L14703, doi:10.1029/2005GL022760.
- van den Dool, H. M., P. Peng, A. Johansson, M. Chelliah, A. Shabbar, and S. Saha, 2006: Seasonal-to-decadal predictability and prediction of North American climate—The Atlantic influence. *J. Climate*, **19**, 6005–6024.
- Wang, B., R. Wu, and K. M. Lau, 2001: Interannual variability of the Asian summer monsoon: Contrasts between the Indian and the western North Pacific–East Asian monsoons. *J. Climate*, **14**, 4073–4090.
- , I.-S. Kang, and J.-Y. Li, 2004: Ensemble simulation of Asian–Australian monsoon variability by 11 AGCMs. *J. Climate*, **17**, 803–818.
- , Q. Ding, X. Fu, I.-S. Kang, K. Jin, J. Shukla, and F. Doblas-Reyes, 2005: Fundamental challenge in simulation and prediction of summer monsoon rainfall. *Geophys. Res. Lett.*, **32**, L15711, doi:10.1029/2005GL022734.
- Wang, W., S. Saha, H.-L. Pan, S. Nadiga, and G. White, 2005: Simulation of ENSO in the new NCEP coupled forecast system model (CFS03). *Mon. Wea. Rev.*, **133**, 1574–1593.
- , M. Chen, and A. Kumar, 2010: An assessment of the CFS real-time seasonal forecasts. *Wea. Forecasting*, **25**, 950–969.
- Webster, P. J., V. O. Magana, T. N. Palmer, J. Shukla, R. A. Tomas, M. Yanai, and T. Yasunari, 1998: Monsoons: Processes, predictability, and the prospects for prediction. *J. Geophys. Res.*, **103**, 14 451–14 510.
- , A. M. Moor, J. P. Loschnigg, and R. R. Leben, 1999: Coupled ocean–atmosphere dynamics in the Indian Ocean during 1997–98. *Nature*, **401**, 356–360.
- Wu, R., and B. P. Kirtman, 2004: Impacts of the Indian Ocean on the Indian summer monsoon–ENSO relationship. *J. Climate*, **17**, 3037–3054.

- , and —, 2005: Roles of Indian and Pacific Ocean air–sea coupling in tropical atmospheric variability. *Climate Dyn.*, **25**, 155–170.
- , and S.-W. Yeh, 2010: A further study of the tropical Indian Ocean asymmetric mode in boreal spring. *J. Geophys. Res.*, **115**, D08101, doi:10.1029/2009JD012999.
- , B. P. Kirtman, and K. Pegion, 2006: Local air–sea relationship in observations and model simulations. *J. Climate*, **19**, 4914–4932.
- , —, and V. Krishnamurthy, 2008: An asymmetric mode of tropical Indian Ocean rainfall variability in boreal spring. *J. Geophys. Res.*, **113**, D05104, doi:10.1029/2007JD009316.
- Yu, J.-Y., C. R. Mechoso, J. C. McWilliams, and A. Arakawa, 2002: Impacts of Indian Ocean on ENSO cycles. *Geophys. Res. Lett.*, **29**, 1204, doi:10.1029/2001GL014098.
- Zhang, C., 1993: Large-scale variability of atmospheric deep convection in relation to sea surface temperature in the tropics. *J. Climate*, **6**, 1898–1913.